EP Detection with Banded Approximation for Unitary-Spread OFDM in Doubly Selective Channels

Zhuangzhuang Liao*†, Jichao Chen†, Zunqi Li*, Xiaojie Fang*‡, Xuejun Sha*, and Dirk Slock†
*Communication Research Center, Harbin Institute of Technology, Harbin, China
†Communication Systems Department, Eurecom, Biot, France
‡National Key Laboratory of Spatial Intelligent Manipulation Technology, Harbin Institute of Technology, Harbin, China
Email: {Liao.Zhuangzhuang, Jichao.Chen, Dirk.Slock}@eurecom.fr,
lizunqi@stu.hit.edu.cn, {fangxiaojie, shaxuejun}@hit.edu.cn

***Abstract*—Unitary-spread OFDM, such as DFT-spread OFDM, improves robustness to frequency selectivity by spreading each data symbol across all active subcarriers. However, in doubly selective channels with fractional Doppler, inter-carrier interference (ICI) makes the effective channel difficult to diagonalize, so high-performance detection becomes computationally demanding. This paper develops a low-complexity expectation propagation (EP) detector that performs cross-domain iterative message passing between the modulation domain and the frequency domain. Exploiting the fact that fractional-Doppler-induced ICI is largely concentrated around the main diagonal of the effective frequency-domain channel, we introduce a banded approximation and incorporate it into the EP update via banded LDU factorization. Simulation results show that the proposed banded EP substantially outperforms linear minimum mean-square error (LMMSE) and closely approaches a dense full-EP reference with a small half-bandwidth, e.g., $B = 2$ in the considered setup, providing an attractive performance–complexity tradeoff.**

***Index Terms*—Banded approximation, expectation propagation, doubly selective channels, unitary-spread OFDM, cross-domain iterative detection**

I. Introduction

High-mobility and wideband links envisioned for 5G-Advanced and beyond often experience doubly selective channels in both delay and Doppler domains [1]. Fractional Doppler breaks subcarrier orthogonality and produces inter-carrier interference (ICI), making the effective frequency-domain channel non-diagonal and classical one-tap equalization insufficient.

Unitary-spread OFDM, such as DFT-spread OFDM (DFT-s-OFDM), is a practical waveform with favorable peak-to-average power ratio (PAPR), robustness to frequency selectivity, and support in modern cellular standards [2]. Tailored frequency-domain processing can reduce equalization complexity in DFT-s-OFDM [3]. Nevertheless, strong Doppler spreads yield residual ICI, calling for detectors that incorporate ICI explicitly while remaining computationally feasible.

Linear receivers such as LMMSE are attractive for their simplicity, but they exploit only second-order statistics and do not explicitly enforce the discrete constellation prior. At the other extreme, exact Maximum Likelihood (ML) detection over coupled subcarriers is prohibitively complex. EP and related expectation-consistency (EC) methods strike a useful middle ground by combining the linear Gaussian observation model with discrete symbol priors via moment matching, and have achieved strong performance in large-scale detection and turbo equalization [4]–[7]. However, direct EP on a dense effective channel requires repeated large matrix factorizations and becomes prohibitive as the number of active subcarriers grows.

To mitigate the complexity bottleneck, structured processing that exploits matrix structure has attracted increasing attention [8]. Banded or block-banded equalization becomes effective when dominant coupling concentrates around the main diagonal [9]. In parallel, cross-domain iterative detection, well-studied for orthogonal time-frequency space (OTFS), alternates between domains where the observation model and symbol prior are naturally expressed, leading to efficient detectors with strong performance [10], [11]. These ideas suggest that retaining only a limited number of dominant couplings and iterating soft information across domains can yield a favorable performance–complexity tradeoff.

In this work, we develop an EP-based detector for unitary-spread OFDM in doubly selective channels. The proposed receiver performs cross-domain iterative inference between the modulation and frequency domains, and incorporates a banded approximation of the effective frequency-domain channel to enable efficient Gaussian updates. By keeping only a small number of dominant off-diagonal couplings, the EP update can be implemented via banded factorizations rather than full dense inversions, thereby reducing complexity while preserving most performance gains from iterative probabilistic detection.

II. System Model

A. Transceiver Model for Unitary-Spread OFDM

We consider block-based multicarrier transmission over N subcarriers, where only N_d subcarriers are active for data and

N_{g} subcarriers on each side are reserved as guard bands, i.e., $N = N_{\mathrm{d}} + 2N_{\mathrm{g}}$.

Let $\mathbf{x} \in \mathbb{C}^{N_{\mathrm{d}}\times 1}$ denote a block of data symbols drawn from a given modulation constellation. At the transmitter, unitary spreading is applied as a linear precoding operation,

$$\mathbf{s} = \mathbf{U}_{N_{\mathrm{d}}}\mathbf{x}, \tag{1}$$

where $\mathbf{U}_{N_{\mathrm{d}}} \in \mathbb{C}^{N_{\mathrm{d}}\times N_{\mathrm{d}}}$ denotes the normalized N_{d}-point unitary transform matrix. Choosing $\mathbf{U}_{N_{\mathrm{d}}}$ as the normalized N_{d}-point DFT yields conventional DFT-s-OFDM.

To enforce the frequency guard bands, the spread vector $\mathbf{s} \in \mathbb{C}^{N_{\mathrm{d}}\times 1}$ is embedded into the N-dimensional frequency grid by zero padding on both sides. Specifically, we define an embedding matrix $\mathbf{J} \in \{0,1\}^{N\times N_{\mathrm{d}}}$ that inserts $\mathbf{s}$ onto the N_{d} central subcarriers and assigns zeros to the $2N_{\mathrm{g}}$ guard subcarriers, yielding

$$\mathbf{x}_{\mathrm{f}} = \mathbf{J}\mathbf{s} \in \mathbb{C}^{N\times 1}. \tag{2}$$

The corresponding time-domain transmit block is obtained via an N-point inverse DFT as

$$\mathbf{x}_{\mathrm{t}} = \mathbf{F}_N^{\mathrm{H}}\mathbf{x}_{\mathrm{f}} = \mathbf{F}_N^{\mathrm{H}}\mathbf{J}\mathbf{s} = \mathbf{F}_N^{\mathrm{H}}\mathbf{J}\mathbf{U}_{N_{\mathrm{d}}}\mathbf{x}, \tag{3}$$

where $\mathbf{F}_N$ denotes the normalized N-point DFT matrix. Finally, a cyclic prefix (CP) of length N_{cp} is appended to each transmit block in order to mitigate the interference caused by multipath propagation.

At the receiver, after cyclic prefix removal and assuming a sufficiently long CP, the resulting length-N block can be expressed as

$$\mathbf{y} = \mathbf{H}_t\mathbf{x}_{\mathrm{t}} + \mathbf{w}, \tag{4}$$

where $\mathbf{H}_t \in \mathbb{C}^{N\times N}$ is the time-domain channel matrix and $\mathbf{w} \sim \mathcal{CN}(\mathbf{0}, \sigma^2\mathbf{I})$ denotes circularly symmetric complex Gaussian white noise. Applying an N-point DFT yields

$$\mathbf{y}_{\mathrm{f}} = \mathbf{F}_N\mathbf{y}. \tag{5}$$

The data-bearing subcarriers are then extracted by the matrix $\mathbf{J}^{\mathrm{H}}$, i.e.,

$$\mathbf{r} = \mathbf{J}^{\mathrm{H}}\mathbf{y}_{\mathrm{f}} \in \mathbb{C}^{N_{\mathrm{d}}\times 1}. \tag{6}$$

B. Doubly Selective Channel Model

We consider a linear time-varying multipath channel with L propagation paths. The continuous-time baseband impulse response is modeled as

$$h(t,\tau) = \sum_{\ell=1}^{L} \alpha_\ell\, \delta(\tau - \tau_\ell)\, e^{j2\pi\nu_\ell t}, \tag{7}$$

where α_ℓ, τ_ℓ, and ν_ℓ denote the complex gain, propagation delay, and Doppler shift associated with the ℓ-th path, respectively.

Block-based transmission with N time-domain samples per block and sampling interval T_s is adopted, such that the block duration is $T = NT_s$. Let Δf denote the subcarrier spacing. The corresponding delay-Doppler resolutions are given by

$$\Delta\tau = \frac{1}{N\Delta f}, \qquad \Delta\nu = \frac{1}{T}. \tag{8}$$

Accordingly, the delay and Doppler parameters of the ℓ-th path can be parameterized as

$$\tau_\ell = \frac{d_\ell + \delta_\ell}{N\Delta f}, \qquad \nu_\ell = \frac{D_\ell + \epsilon_\ell}{T}, \tag{9}$$

where $d_\ell, D_\ell \in \mathbb{Z}$ denote the integer delay and Doppler indices, and $\delta_\ell, \epsilon_\ell \in (-0.5, 0.5]$ represent the corresponding fractional components.

The discrete-time channel matrix can be written as a superposition of delay and Doppler operators,

$$\mathbf{H}_t = \sum_{\ell=1}^{L} \alpha_\ell\, \boldsymbol{\Delta}(\nu_\ell)\, \boldsymbol{\Pi}(\tau_\ell), \tag{10}$$

where the Doppler operator is defined as the diagonal modulation matrix

$$\boldsymbol{\Delta}(\nu_\ell) = \mathrm{diag}\Big(e^{j2\pi\nu_\ell nT_s}\Big)_{n=0}^{N-1}, \tag{11}$$

and the delay operator is expressed in the frequency domain as

$$\boldsymbol{\Pi}(\tau_\ell) = \mathbf{F}_N^{\mathrm{H}}\, \mathrm{diag}\Big(e^{-j2\pi k\Delta f\tau_\ell}\Big)_{k=0}^{N-1} \mathbf{F}_N. \tag{12}$$

Integer delays reduce to circular sample shifts, while fractional delays cause spectral leakage and inter-delay interference.

In wideband/low-latency settings, the block duration T is small, so the Doppler resolution $\Delta\nu = 1/T$ is coarse. Under practical mobility, Doppler is often dominated by the fractional component (typically $D_\ell = 0$), which is the regime considered in this paper.

III. Cross-domain EP with Banded Approximation

A. Equivalent Frequency-Domain Channel and Banded Approximation

Based on the transceiver structure described in the previous section, the detection problem is formulated in the frequency domain after subcarrier extraction. Specifically, after CP removal, DFT operation, and removal of guard subcarriers, the observation vector can be written as

$$\mathbf{r} = \mathbf{J}^{\mathrm{H}}\mathbf{F}_N\mathbf{H}_t\mathbf{F}_N^{\mathrm{H}}\mathbf{J}\,\mathbf{s} + \mathbf{J}^{\mathrm{H}}\mathbf{F}_N\mathbf{w}, \tag{13}$$

where $\mathbf{s} \in \mathbb{C}^{N_{\mathrm{d}}\times 1}$ denotes the spread symbol vector and $\mathbf{J}$ is the subcarrier embedding matrix. The effective frequency-domain channel is thus given by

$$\mathbf{H}_{\mathrm{f}} = \mathbf{J}^{\mathrm{H}}\mathbf{F}_N\mathbf{H}_t\mathbf{F}_N^{\mathrm{H}}\mathbf{J} \in \mathbb{C}^{N_{\mathrm{d}}\times N_{\mathrm{d}}}. \tag{14}$$

By substituting $\boldsymbol{\Pi}(\tau_\ell) = \mathbf{F}_N^{\mathrm{H}}\mathrm{diag}(e^{-j2\pi k\Delta f\tau_\ell})\mathbf{F}_N$, one obtains

$$\mathbf{F}_N\boldsymbol{\Delta}(\nu_\ell)\boldsymbol{\Pi}(\tau_\ell)\mathbf{F}_N^{\mathrm{H}} = \underbrace{\left(\mathbf{F}_N\boldsymbol{\Delta}(\nu_\ell)\mathbf{F}_N^{\mathrm{H}}\right)}_{\mathbf{G}(\nu_\ell)}\, \mathrm{diag}\Big(e^{-j2\pi k\Delta f\tau_\ell}\Big), \tag{15}$$

indicating that Doppler dispersion determines the inter-carrier interference amplitude, while delay mainly contributes a frequency-dependent phase rotation.

Define $\mathbf{G}(\nu_\ell) \triangleq \mathbf{F}_N\boldsymbol{\Delta}(\nu_\ell)\mathbf{F}_N^{\mathrm{H}}$. Its (p,q)-th entry is

$$[\mathbf{G}(\nu_\ell)]_{p,q} = \frac{1}{N}\sum_{n=0}^{N-1} e^{j2\pi\nu_\ell nT_s}\, e^{-j2\pi(p-q)\frac{n}{N}}. \tag{16}$$

In the fractional-Doppler regime where $D_\ell = 0$ (hence $\nu_\ell = \epsilon_\ell/T$ and $T = NT_s$), this entry becomes a Dirichlet kernel

$$[\mathbf{G}(\nu_\ell)]_{p,q} = \frac{1}{N}\sum_{n=0}^{N-1} e^{j2\pi(\epsilon_\ell-(p-q))\frac{n}{N}} \triangleq \mathcal{D}_N(\epsilon_\ell-(p-q))\,. \tag{17}$$

For $x \not\equiv 0 \pmod N$, the magnitude can be expressed and upper bounded as

$$|\mathcal{D}_N(x)| = \left|\frac{\sin(\pi x)}{N\sin(\pi x/N)}\right| \le \frac{1}{N\,|\sin(\pi x/N)|}. \tag{18}$$

The function $\mathcal{D}_N(\cdot)$ exhibits a pronounced main lobe around $p-q \approx \epsilon_\ell$ and rapidly decaying sidelobes as $|p-q|$ increases. As a result, the dominant inter-carrier coupling induced by fractional Doppler is concentrated in the vicinity of the main diagonal of the frequency-domain channel matrix.

This structural property motivates a banded approximation with half-bandwidth B:

$$[\mathbf{H}_{\mathrm{f}}^{(B)}]_{p,q} = \begin{cases}[\mathbf{H}_{\mathrm{f}}]_{p,q}, & |p-q| \le B,\\ 0, & \text{otherwise.}\end{cases} \tag{19}$$

Increasing B reduces the discarded out-of-band energy and improves the accuracy of the approximation. The banded structure enables efficient LDU-based updates and avoids full-matrix operations; thus we use $\mathbf{H}_{\mathrm{f}}^{(B)}$ in the proposed EP detector.

B. Cross-Domain EP Detection

Based on the banded approximation developed in the previous section, the detection problem can be formulated in the frequency domain as the linear model

$$\mathbf{r} \approx \mathbf{H}_{\mathrm{f}}^{(B)}\mathbf{s} + \mathbf{w}', \tag{20}$$

where $\mathbf{w}' = \mathbf{J}^{\mathrm{H}}\mathbf{F}_N\mathbf{w} \sim \mathcal{CN}(\mathbf{0}, \sigma^2\mathbf{I})$.

The detection problem involves two coupled domains: a linear Gaussian observation model in the frequency domain and a discrete symbol prior in the modulation domain. The joint probability density function can be factorized as

$$p(\mathbf{r},\mathbf{s},\mathbf{x}) = p(\mathbf{r}\mid\mathbf{s})\,p(\mathbf{s}\mid\mathbf{x})\,p(\mathbf{x}), \tag{21}$$

and the corresponding factor functions are

$$\Psi_r \triangleq p(\mathbf{r}\mid\mathbf{s}) = \mathcal{CN}\Big(\mathbf{r};\,\mathbf{H}_{\mathrm{f}}^{(B)}\mathbf{s},\,\sigma^2\mathbf{I}\Big)\,, \tag{22}$$

$$\Psi_s \triangleq p(\mathbf{s}\mid\mathbf{x}) = \delta(\mathbf{s}-\mathbf{U}_{N_{\mathrm{d}}}\mathbf{x})\,, \tag{23}$$

$$\Psi_x \triangleq p(\mathbf{x}) = \prod_{n=1}^{N_{\mathrm{d}}} p(x_n). \tag{24}$$

(1): Consider the symbol node x_n associated with the discrete prior factor Ψ_x. The incoming message from the spreading constraint factor Ψ_s is denoted by

$$m_{\Psi_s\to x_n}(x_n) \propto \mathcal{CN}(x_n;\mu_{s\to x_n},\,\nu_{s\to x_n})\,. \tag{25}$$

Within EP, the message from the symbol node x_n back to the spreading constraint factor Ψ_s is obtained via moment matching,

$$m_{x_n\to\Psi_s}(x_n) \propto \frac{\mathrm{Proj}[p(x_n)\,m_{\Psi_s\to x_n}(x_n)]}{m_{\Psi_s\to x_n}(x_n)}. \tag{26}$$

Here $\mathrm{Proj}[\cdot]$ denotes Gaussian projection by matching the first two moments.

(2): Collecting the Gaussian messages from all symbol nodes yields

$$m_{x\to\Psi_s}(\mathbf{x}) = \prod_{n=1}^{N_{\mathrm{d}}} m_{x_n\to\Psi_s}(x_n) = \mathcal{CN}(\mathbf{x};\,\boldsymbol{\mu}_x,\,\mathbf{C}_x)\,, \tag{27}$$

where $\mathbf{C}_x = \mathrm{diag}(\nu_{x_1},\dots,\nu_{x_{N_{\mathrm{d}}}})$. Through the unitary spreading relation, the message induced by Ψ_s on the frequency-domain variable $\mathbf{s}$ is obtained as

$$m_{\Psi_s\to s}(\mathbf{s}) = \mathcal{CN}(\mathbf{s};\,\boldsymbol{\mu}_s,\,\mathbf{C}_s)\,, \tag{28}$$

with

$$\boldsymbol{\mu}_s = \mathbf{U}_{N_{\mathrm{d}}}\,\boldsymbol{\mu}_x, \tag{29}$$

$$\mathbf{C}_s = \mathbf{U}_{N_{\mathrm{d}}}\,\mathbf{C}_x\,\mathbf{U}_{N_{\mathrm{d}}}^{\mathrm{H}}. \tag{30}$$

In general, $\mathbf{C}_s$ is dense. For computational tractability in the subsequent frequency-domain update, it is approximated by a scalar-variance model

$$\mathbf{C}_s \approx \nu_s\,\mathbf{I}, \qquad \nu_s \triangleq \frac{1}{N_{\mathrm{d}}}\mathrm{tr}(\mathbf{C}_s) = \frac{1}{N_{\mathrm{d}}}\sum_{n=1}^{N_{\mathrm{d}}}\nu_{x_n}. \tag{31}$$

(3): The incoming message from $\mathbf{s}$ to Ψ_r is then approximated as

$$m_{s\to\Psi_r}(\mathbf{s}) = m_{\Psi_s\to s}(\mathbf{s}) = \mathcal{CN}(\mathbf{s};\,\boldsymbol{\mu}_s,\,\nu_s\,\mathbf{I})\,. \tag{32}$$

Combining the observation factor with the incoming message yields

$$q(\mathbf{s}) \propto \Psi_r(\mathbf{s})\,m_{s\to\Psi_r}(\mathbf{s}) = \mathcal{CN}\big(\mathbf{s};\,\boldsymbol{\mu}_s^{\mathrm{post}},\,\mathbf{C}_s^{post}\big)\,, \tag{33}$$

where the posterior mean and covariance are given by

$$\mathbf{C}_s^{\mathrm{post}} = \left(\frac{1}{\nu_s}\mathbf{I} + \frac{1}{\sigma^2}\mathbf{H}_{\mathrm{f}}^{(B)\mathrm{H}}\mathbf{H}_{\mathrm{f}}^{(B)}\right)^{-1}, \tag{34}$$

$$\boldsymbol{\mu}_s^{\mathrm{post}} = \mathbf{C}_s^{post}\left(\frac{1}{\nu_s}\boldsymbol{\mu}_s + \frac{1}{\sigma^2}\mathbf{H}_{\mathrm{f}}^{(B)\mathrm{H}}\mathbf{r}\right). \tag{35}$$

Since $\mathbf{H}_{\mathrm{f}}^{(B)}$ is banded, the linear system in (35) (and the required diagonal terms of $\mathbf{C}_s^{post}$) can be computed efficiently using a banded LDU factorization and forward/back substitutions.

Following the EP principle, the message from the observation factor Ψ_r back to the variable node $\mathbf{s}$ is obtained by

$$m_{\Psi_r\to s}(\mathbf{s}) \propto \frac{q(\mathbf{s})}{m_{s\to\Psi_r}(\mathbf{s})} = \mathcal{CN}(\mathbf{s};\,\boldsymbol{\mu}_{r\to s},\,\mathbf{C}_{r\to s})\,, \tag{36}$$

with (component-wise)

$$[\mathbf{C}_{r\to s}]_{n,n} = \left(\frac{1}{[\mathbf{C}_s^{\mathrm{post}}]_{n,n}} - \frac{1}{\nu_s}\right)^{-1}, \tag{37}$$

$$[\boldsymbol{\mu}_{r\to s}]_n = [\mathbf{C}_{r\to s}]_{n,n}\left(\frac{[\boldsymbol{\mu}_s^{\mathrm{post}}]_n}{[\mathbf{C}_s^{\mathrm{post}}]_{n,n}} - \frac{[\boldsymbol{\mu}_s]_n}{\nu_s}\right). \tag{38}$$

(4): Since $\mathbf{s}$ is connected only to Ψ_r and Ψ_s, $m_{s\to\Psi_s}(\mathbf{s}) = m_{\Psi_r\to s}(\mathbf{s})$. The message induced by Ψ_s on the symbol-domain variable $\mathbf{x}$ is obtained by a linear transformation of the Gaussian message,

$$m_{\Psi_s\to x}(\mathbf{x}) = \mathcal{CN}(\mathbf{x};\,\boldsymbol{\mu}_{s\to x},\,\mathbf{C}_{s\to x})\,, \tag{39}$$

with

$$\boldsymbol{\mu}_{s\to x} = \mathbf{U}_{N_{\mathrm{d}}}^{\mathrm{H}}\,\boldsymbol{\mu}_{r\to s}, \tag{40}$$

$$\mathbf{C}_{s\to x} = \mathbf{U}_{N_{\mathrm{d}}}^{\mathrm{H}}\,\mathbf{C}_{r\to s}\,\mathbf{U}_{N_{\mathrm{d}}}. \tag{41}$$

For subsequent symbol-wise EP processing in (25), $\mu_{s\to x_n}$ and $\nu_{s\to x_n}$ are extracted from the mean vector (40) and the diagonal entries of (41), respectively.

C. Complexity and Convergence Discussion

Computational Complexity: The dominant computations in each EP iteration arise from the frequency-domain update at the observation factor Ψ_r, i.e., the evaluation of $\boldsymbol{\mu}_s^{post}$ and the required diagonal terms of $\mathbf{C}_s^{post}$ in (34)–(35). Since $\mathbf{H}_\mathrm{f}^{(B)}$ is banded with half-bandwidth B, the Gram matrix $\mathbf{H}_\mathrm{f}^{(B)\mathrm{H}}\mathbf{H}_\mathrm{f}^{(B)}$ remains banded with half-bandwidth on the order of $2B$. Therefore, solving for $\boldsymbol{\mu}_s^{post}$ via a banded LDU factorization has per-iteration complexity on the order of $\mathcal{O}(N_\mathrm{d}B^2)$. In contrast, dense full EP requires a dense factorization with per-iteration complexity $\mathcal{O}(N_\mathrm{d}^3)$. The remaining operations (unitary transforms and symbol-wise EP updates) are of lower order and do not dominate for moderate B.

In addition, the extrinsic computation in (38) requires only diagonal entries. Following the idea in [12], [13], rather than computing the full diagonal entries, we approximate it using a single representative diagonal element. This avoids additional matrix-inverse-related computations beyond the banded solve used for $\boldsymbol{\mu}_s^{post}$, thereby keeping the overall complexity essentially unchanged and still dominated by the banded LDU factorization.

Convergence Stabilization: To improve robustness, we adopt two standard stabilization techniques, following [6].

1) Damping: We apply $(\mu,\nu) \leftarrow (1-\beta)(\mu^{\mathrm{old}},\nu^{\mathrm{old}}) + \beta(\mu^{\mathrm{new}},\nu^{\mathrm{new}})$ with $\beta \in (0,1]$, where β is the damping factor. A smaller β generally improves stability at the expense of slower convergence.

2) Minimum variance threshold: To prevent negative or excessively small variances, we enforce a variance floor $\nu \leftarrow \max(\nu,\nu_{\min})$ with a prescribed $\nu_{\min} > 0$.

IV. Simulation

A. Simulation Setup

We consider a block-based DFT-spread OFDM transmission with a total of $N = 512$ subcarriers and subcarrier spacing $\Delta f = 15$ kHz. To accommodate spectral shaping and mitigate edge effects, guard subcarriers are reserved on both sides with $N_\mathrm{g} = 32$ subcarriers, such that the number of data subcarriers is $N_\mathrm{d} = N - 2N_\mathrm{g} = 448$. QPSK modulation is employed, and the proposed EP detector runs for at most $I_{\max} = 10$ iterations. The CP length is chosen to exceed the maximum delay spread.

The wireless channel follows a doubly selective delay-Doppler model with fractional delay and fractional Doppler parameters. Specifically, $L = 5$ independent propagation paths are assumed. The maximum excess path length is set to $\Delta d_{\max} = 400$ m (corresponding to a maximum delay of $\tau_{\max} = \Delta d_{\max}/c$), where c denotes the speed of light, and the maximum speed is $v_{\max} = 300$ km/h with carrier frequency $f_c = 6$ GHz. We compare LMMSE, EP with banded approximation ($B = 0$ and $B = 2$), and EP without banding (dense full-EP).

B. Simulation Results and Analysis

Fig. 1 reports the bit error rate (BER) versus signal-to-noise ratio (SNR). As a performance baseline, the LMMSE detector

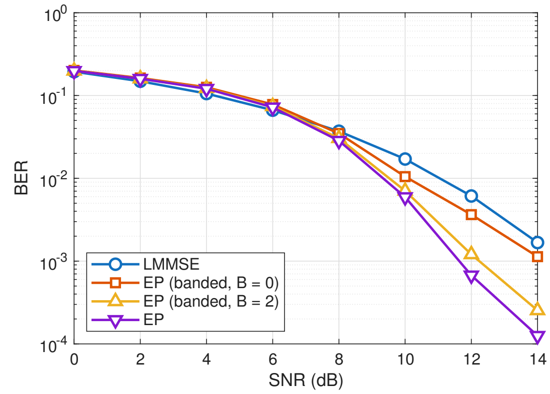

Fig. 1. BER versus SNR for LMMSE, EP with banded approximation ($B = 0$ and $B = 2$), and dense full-EP in a doubly selective channel.

is included for comparison. When $\mathrm{SNR} < 6$ dB, thermal noise dominates and the linear LMMSE solution is relatively robust, whereas the Gaussian projection and band truncation used by EP can introduce slight model mismatch. As SNR increases, residual structured ICI becomes the main impairment, so EP better exploits the discrete prior and iterative interference refinement. This operating region is of primary practical interest since typical communication links are designed to work above about 6 dB to meet target reliability requirements.

The half-bandwidth B controls the performance–complexity tradeoff. With $B = 0$, only the main diagonal is retained and the gain over LMMSE is modest. Increasing B improves ICI modeling, and in the considered setup a small half-bandwidth, e.g., $B = 2$, can recover most of the benefit of dense full EP at low complexity.

V. Conclusion

This paper proposes a low-complexity cross-domain EP detector for unitary-spread OFDM in doubly selective channels. By leveraging the near-banded structure of the effective frequency-domain channel induced by fractional Doppler, a banded approximation was introduced to enable efficient banded LDU-based updates within EP. Simulation results demonstrated that the proposed banded-EP achieves substantial BER gains over LMMSE and approaches the dense full-EP reference while using a small half-bandwidth, e.g., $B = 2$ in the considered setup, providing an attractive performance–complexity tradeoff for high-mobility transmissions.

Acknowledgment

Harbin Institute of Technology's research is partially supported by the Key Program of the National Natural Science Foundation of China under Grant U23A20278 and by the independent research project of the National Key Laboratory of Spatial Intelligent Manipulation Technology.

EURECOM's research is partially supported by its industrial members: ORANGE, BMW, SAP, iABG, Norton LifeLock, by the Franco-German projects CellFree6G, the French PEPR-5G projects PERSEUS and YACARI, the EU H2030 RI project CONVERGE, and by a Huawei France funded Chair towards Future Wireless Networks.

References

[1] R. Bomfin, M. Chafii, A. Nimr, and G. Fettweis, "A Robust Baseband Transceiver Design for Doubly-Dispersive Channels," *IEEE Transactions on Wireless Communications*, vol. 20, no. 8, pp. 4781–4796, 2021.

[2] 3rd Generation Partnership Project (3GPP), "NR; Physical channels and modulation," 3GPP, Technical Specification TS 38.211, Apr. 2025, release 18, v18.6.0.

[3] J. Chae, J. Choi, J. Kim, and J. H. Cho, "A Low-Complexity Widely-Linear MMSE Equalizer for DFT-Spread OFDM With Frequency-Domain Spectrum Shaping," *IEEE Transactions on Wireless Communications*, vol. 23, no. 4, pp. 3465–3479, 2024.

[4] J. Céspedes, P. M. Olmos, M. Sánchez-Fernández, and F. Perez-Cruz, "Probabilistic MIMO Symbol Detection With Expectation Consistency Approximate Inference," *IEEE Transactions on Vehicular Technology*, vol. 67, no. 4, pp. 3481–3494, 2018.

[5] H. Wang, A. Kosasih, C.-K. Wen, S. Jin, and W. Hardjawana, "Expectation Propagation Detector for Extra-Large Scale Massive MIMO," *IEEE Transactions on Wireless Communications*, vol. 19, no. 3, pp. 2036–2051, 2020.

[6] I. Santos, J. J. Murillo-Fuentes, R. Boloix-Tortosa, E. Arias-de Reyna, and P. M. Olmos, "Expectation Propagation as Turbo Equalizer in ISI Channels," *IEEE Transactions on Communications*, vol. 65, no. 1, pp. 360–370, 2017.

[7] I. Santos, J. J. Murillo-Fuentes, J. C. Aradillas, and E. Arias-De-Reyna, "Channel Equalization With Expectation Propagation at Smoothing Level," *IEEE Transactions on Communications*, vol. 68, no. 5, pp. 2740–2747, 2020.

[8] A.-J. v. der Veen, J. Romme, and Y. Cui, "Rank Detection Thresholds for Hankel or Toeplitz Data Matrices," in *2020 28th European Signal Processing Conference (EUSIPCO)*, 2021, pp. 1911–1915.

[9] A. Ancora, G. Montalbano, and D. T. M. Slock, "Performance Analysis of Preconditioned Iterative Inter-Carrier Interference Cancellation for OFDM," in *2010 IEEE International Conference on Communications*, 2010, pp. 1–5.

[10] S. Li, W. Yuan, Z. Wei, and J. Yuan, "Cross Domain Iterative Detection for Orthogonal Time Frequency Space Modulation," *IEEE Transactions on Wireless Communications*, vol. 21, no. 4, pp. 2227–2242, 2022.

[11] R. Chong, S. Li, Z. Wei, M. Matthaiou, D. W. K. Ng, and G. Caire, "Cross-Domain Iterative Detection for OTFS Transmission With Frequency Domain Equalization," *IEEE Transactions on Communications*, vol. 73, no. 10, pp. 9886–9902, 2025.

[12] Z. Li, C. Zhang, G. Song, X. Fang, X. Sha, and D. T. M. Slock, "Chirp Parameter Selection for Affine Frequency Division Multiplexing With MMSE Equalization," *IEEE Transactions on Communications*, vol. 73, no. 7, pp. 5079–5093, 2025.

[13] S. Omar, A. Ancora, and D. T. Slock, "Performance analysis of general pilot-aided linear channel estimation in LTE OFDMA systems with application to simplified MMSE schemes," in *2008 IEEE 19th International Symposium on Personal, Indoor and Mobile Radio Communications*, 2008, pp. 1–6.